IOP Publishing Phys. Med. Biol. 65 (2020) 075011 (12pp) https://doi.org/10.1088/1361-6560/ab730a

Physics in Medicine & Biology

IPEM Institute of Physics and Engineering in Medicine

PAPER

On the concepts of dose-mean lineal energy, unrestricted and restricted dose-averaged LET in proton therapy

A Bertolet[1,2], M A Cortés-Giraldo[2] and A Carabe-Fernandez[1,3]

[1] Department of Radiation Oncology, Hospital of The University of Pennsylvania, Philadelphia, PA, United States of America
[2] Department of Atomic, Molecular and Nuclear Physics, Universidad de Sevilla, Seville, Spain
[3] Author to whom any correspondence should be addressed.

E-mail: a.carabe@uphs.upenn.edu **and** alexcarabe@gmail.com

RECEIVED
1 October 2019

REVISED
26 January 2020

ACCEPTED FOR PUBLICATION
5 February 2020

PUBLISHED
2 April 2020

Keywords: microdosimetry, LET, lineal energy, proton therapy, y_D calculation, restricted LET, LETd calculation

Abstract

To calculate 3D distributions of microdosimetric-based restricted dose-averaged LET (LETd) and dose-mean lineal energy (y_D) in order to explore their similarities and differences between each other and with the traditional unrestricted LETd. Additionally, a new expression for optimum restricted LETd calculation is derived, allowing for disregarding straggling-associated functions in the classical microdosimetric theory.

Restricted LETd and y_D for polyenergetic beams can be obtained by integrating previously developed energy-dependent microdosimetric functions over the energetic spectrum of these beams. This calculation is extended to the entire calculation volume using an algorithm to determine spectral fluence. Equivalently, unrestricted LETd can be obtained integrating the stopping power curve on the spectrum. A new expression to calculate restricted LETd is also derived. Results for traditional and new formulas are compared for a clinical 100 MeV proton beam. Distributions of unrestricted LETd, restricted LETd and y_D are analyzed for a prostate case, for microscopic spherical sites of 1 μm and 10 μm in diameter.

Traditional and new expressions for restricted LETd remarkably agree, being the mean differences 0.05 ± 0.04 keV μm^{-1} for the 1 μm site and 0.05 ± 0.02 keV μm^{-1} for the 10 μm site. In the prostate case, the ratio between the maximum and the central value for central axis (CAX) profiles is around 2 for all the quantities, being the highest for restricted LETd for 1 μm (2.17) and the lowest for y_D for 1 μm (1.78).

Unrestricted LETd, restricted LETd and y_D can be analytically computed and compared for clinical plans. Two important consequences of the calculation of y_D are: (1) its distribution can be verified by directly measuring it in clinical beams; and (2), optimization of proton treatments based on these quantities is enabled as well as future developments of RBE models based on them.

Introduction

The importance of the biophysical properties of proton therapy beams have been substantially considered due to the variability of the relative biological effectiveness (RBE) (Paganetti 2014, Paganetti *et al* 2019) and its potential clinical consequences. The use of intensity modulated techniques in proton therapy (IMPT) is becoming the standard of care, and these types of techniques produce non-homogeneous dose-averaged LET (LETd) distributions (Grassberger *et al* 2011) that have been shown to be correlated with clinical outcomes (Peeler *et al* 2016). While the large variability of RBE *in vitro* experiments makes its determination, in general, indistinguishable from its associated uncertainty (Paganetti 2014), LETd is a physical quantity accurately computable (Romano *et al* 2014, Cortés-Giraldo and Carabe 2015) and directly correlated with RBE. This correlation may lead to a practical biophysical optimization of proton therapy treatments (Giantsoudi *et al* 2013,

Fager *et al* 2015, Unkelbach *et al* 2016, An *et al* 2017, Inaniwa *et al* 2017, Cao *et al* 2018, McMahon and Paganetti 2018, Guan *et al* 2019, Sánchez-Parcerisa *et al* 2019).

The concept of LETd, nonetheless, contains some simplifications and disregards relevant aspects of the patterns of energy imparted in matter. LETd is traditionally calculated by employing data for collision stopping power or unrestricted LET (Wilkens and Oelfke 2003, 2004, Marsolat *et al* 2016, Deng *et al* 2019), which is defined as the mean energy lost by the proton in electronic collision processes per unit path length (ICRU 2016). Nevertheless, to better characterize the concentration or density of energy deposition in biological structures, energy carried out away from them should be taken off this computation. In this context, the concept of restricted LET, L_Δ arises, normally defined by using a threshold kinetic energy for secondary delta-rays, Δ, above which those are disregarded (ICRU 2016). However, in this work the restriction is defined spatially as explained below.

By using the microdosimetry formalism (ICRU 1983, Kellerer *et al* 1985) and the concept of *site*, spatially-restricted LETd can be calculated. Furthermore, the microdosimetric concept of lineal energy (y) and its equivalent version of LETd, called dose-mean lineal energy (y_D) might better represent microscopic distribution of the energy depositions since they contain the information of the imparted energy patterns in small volumes instead of per track length as done with the macroscopic concept of LET. In this sense, y_D has been also related to RBE by means of the Microdosimetric–Kinetic Model (MKM) (Hawkins 1996, 2003) and their subsequent modifications (Kase *et al* 2008, 2013). In fact, efforts have lately been put to establish this connection (Newpower *et al* 2019, Perales *et al* 2019) and enable the biophysical optimization of proton radiotherapy treatments in terms of y_D. Nevertheless, determination of y_D in clinical cases would require extremely lengthy Monte Carlo (MC) simulations down to microscopic level, which has made its use impractical so far.

In previous articles, we have presented models to calculate microdosimetric quantities such as y_D and restricted LETd in monoenergetic beams (Bertolet *et al* 2019a). Independently, we have developed and introduced an analytical algorithm to determine the energetic spectrum for proton therapeutic beams in each voxel inside a calculation volume within a patient (Bertolet *et al* 2020). Here, we combine these two works to produce distributions of restricted LETd and y_D in clinical proton therapy cases. This has led us to propose a simplified and optimized expression for restricted LETd. Analogies and differences between distributions of unrestricted LETd, restricted LETd and y_D are here explored.

Methods and materials

In order to clarify the notation employed throughout this work and make the reading easier, table 1 shows a list of relevant variables, their symbols and their nature.

LET and its relation with microdosimetry

A site is a certain region of interest, with a given shape and size, in a particular medium in which the energy imparted by a particle in its electronic collisions is scored. Each incident charged heavy particle has a defined track, composed of its trajectory as well as those for the secondary electrons generated along its way. An interaction between a track and a site is called event. The amount of energy imparted to the site in a single event is notated by ε_s. This is a stochastic quantity, i.e. it varies from event to event even when the experimental conditions are the same. Therefore, ε_s is characterized by a probability distribution $f(\varepsilon_s)$, with certain mean value $\overline{\varepsilon_s}$ and variance $\sigma^2_{\varepsilon_s}$, which provides a measurement of the variability for the value of ε_s in an experiment. The variability on ε_s is influenced by three sources (Kellerer *et al* 1985): (i) the variability on the *average* energy imparted per unit length, characterized by means of the linear energy transfer (LET), that represents the ability of the particle to interact with the medium (i.e. interaction cross section); (ii) the variability on the segment length s, which is the distance travelled by the particle within the site (Bertolet *et al* 2019a); and (iii) the energy straggling, i.e. given an average energy imparted per unit length, the variability on the number of collisions and energy deposited in them due to stochastic nature of interactions between radiation and matter.

The quotient between the energy imparted in a single event ε_s and the mean segment length $\bar{s}$ of tracks in the site is called lineal energy:

$$y = \frac{\varepsilon_s}{\bar{s}}. \tag{1}$$

Consequently, lineal energy is also a stochastic quantity, characterized by a distribution $f(y)$ that includes information about the volumetric pattern of energy deposition. However, the deterministic concept of LET is generally employed instead, since it allows for a more simplistic approach in which track structure can be disregarded. In this context, when dealing with a polyenergetic or multi-particle beam, a distribution of different values for LET arises. In such a situation, it has been shown (Grassberger and Paganetti 2011) that for typical doses in proton therapy the dose-weighted average or dose-averaged LET, $\bar{L}_D$, is more representative of the biological effect than the simple average LET, traditionally called track-averaged or fluence-averaged LET, $\bar{L}_T$.

Table 1. List of relevant quantities employed in the mathematical development throughout this work, with their symbols and nature. For LET-wise quantities, the combination of the subscripts here shown combine their nature: for example, $\bar{L}_{\Delta,D}$ is the dose-average spatially restricted linear energy transfer.

Symbol	Quantity	Nature
ε_s	Energy imparted per event	Stochastic (event-wise)
$\overline{\varepsilon_s}$	Mean energy imparted per event	Average of distribution of ε_s per event
$\sigma^2_{\varepsilon_s}$	Variance of the energy imparted per event	Variance of distribution of ε_s per event
s	Segment length for an event	Stochastic (event-wise)
$\bar{s}$	Mean segment length	Average of distribution of s per event
$\bar{s}_D$	Weighted-average segment length	Weighted average of distribution of s per event
y	Lineal energy for an event	Stochastic (event-wise)
$\bar{y}_D$	Dose-mean lineal energy	Weighted average of distribution of y per event
ε_c	Energy imparted per collision	Stochastic (collision-wise)
$\overline{\varepsilon_c} \equiv \delta_1$	Mean energy imparted per collision	Average of distribution of ε_c per collision
δ_2	Weighted-average energy imparted per collision	Weighted average of distribution of ε_c per collision
$S(E)$	Stopping power for protons of energy E	Function of proton energy
$\overline{\varepsilon_s}(E)$	Mean energy imparted per event for protons of energy E	Function of proton energy
$\sigma^2_{\varepsilon_s}(E)$	Variance of the energy imparted per event for protons of energy E	Function of proton energy
$\phi_E(E)$	Differential spectrum for a beam: distribution of particles with energy E	Distribution per proton energy
$\overline{\overline{\varepsilon_s}} \equiv \overline{\overline{\varepsilon_s}(E)}$	Average of mean energy imparted per event for a polyenergetic beam	Average of distribution of $\overline{\varepsilon_s}$ per proton energy
$\overline{\sigma^2_{\varepsilon_s}} \equiv \overline{\sigma^2_{\varepsilon_s}(E)}$	Average of the variance of the energy imparted per event for protons of energy E	Average of distribution of $\sigma^2_{\varepsilon_s}$ per proton energy
$\sigma^2_{\overline{\varepsilon_s}} \equiv \sigma^2_{\overline{\varepsilon_s}(E)}$	Variance of the mean energy imparted per event	Variance of distribution of $\overline{\varepsilon_s}$ per proton energy
$\bar{L}_T$	Track-average linear energy transfer	Average of distribution of LET per particle
$\bar{L}_D$	Dose-average linear energy transfer	Weighted average of distribution of LET per particle
L_∞	Unrestricted linear energy transfer	Deterministic
L_Δ	Spatially restricted linear energy transfer	Deterministic

To clarify notation employed hereinafter, any *weighted*-average of stochastic quantity x with distribution $f(x)$ is notated by the subscript D. In other words, $\bar{x}_D$ represents the weighted-average for any stochastic quantity x. For further identification of each variable, see table 1. Dose-averaged restricted LET is related to dose-mean lineal energy $\bar{y}_D$ by Bertolet *et al* (2019a)

$$\bar{L}_{\Delta,D} = \frac{\bar{s}}{\bar{s}_D}\bar{y}_D - \frac{\delta_2}{\bar{s}_D} \tag{2}$$

where $\bar{s}$ and $\bar{s}_D$ are the average and the weighted average of the distribution of segment length, respectively, and δ_2 is the weighted average of the distribution of the energy imparted per electronic collision ε_c (Bertolet *et al* 2019b). Additionally, the subscript Δ is added to $\bar{L}_D$ to indicate that, by using this formalism, the obtained LET is restricted to a site dimension noted by Δ.

In previous works, we have developed analytical functions on the proton energy for the averages and variances of the microdosimetric distributions (Bertolet *et al* 2019a). By using these functions, the mean energy imparted, and the variance of the energy imparted for a polyenergetic proton beam $\sigma^2_{\varepsilon_s,\phi}$ can be obtained, respectively, as

$$\overline{\overline{\varepsilon_s}} = \frac{\int \overline{\varepsilon_s}(E)\ \phi_E(E)\ \mathrm{d}E}{\int \phi_E(E)\ \mathrm{d}E} \tag{3}$$

and

$$\sigma^2_{\varepsilon_s,\phi} = \frac{\int \sigma^2_{\varepsilon_s}(E)\ \phi_E(E)\ dE}{\int \phi_E(E)\ dE} + \frac{\int \left(\overline{\varepsilon_s}(E) - \overline{\overline{\varepsilon_s}}\right)^2 \phi_E(E)\ \mathrm{d}E}{\int \phi_E(E)\ \mathrm{d}E} \tag{4}$$

where $\phi_E(E)$ represents the spectral fluence of the beam as a function of the energy, $\overline{\varepsilon_s}(E)$ and $\sigma^2_{\varepsilon_s}(E)$ are the average and variance of ε_s calculated for monoenergetic protons of energy E. A demonstration for equation (4) is included in the Appendix. Similarly, averages and variances of the overall distributions of segment length s and energy imparted per electronic collision can be obtained. In equation (3) note the double average since the obtained mean energy is the averaged value over the different energies present in the beam, which, in turn, have their own average value for the microdosimetric distribution of energy imparted. Equation (4), on the other hand, is composed by two terms: the first term is the mean variance across the energies present in the beam, $\overline{\sigma^2_{\varepsilon_s}}$, and the second is the variance of the averages of the microdosimetric distributions of energy imparted, $\sigma^2_{\overline{\varepsilon_s}}$.

Unrestricted LETd

Dose-averaged LET can be obtained regardless microdosimetric considerations by employing the concept of collision or electronic stopping power S or unrestricted LET, L_∞, in which the energy lost by the particle in electronic collisions is considered instead of the energy imparted in a certain region as microdosimetry does. Stopping power is a deterministic concept, which means it has no stochastic variability. Therefore, given a particle with energy E, we can note it as

$$S(E) = \frac{d\varepsilon_\infty(E)}{ds} \tag{5}$$

where $d\varepsilon_\infty(E)$ is the mean energy lost by the particle in an infinitesimal distance ds. Note that $d\varepsilon_\infty$ here is a deterministic quantity. As the dose imparted by a particle with a given stopping power S can be considered proportional to S, the dose-averaged electronic stopping power or unrestricted dose-averaged LET can be obtained by weighting the electronic stopping power by itself so that

$$\bar{L}_{\infty,D} = \frac{\int S^2(E)\ \phi_E(E)\ \mathrm{d}E}{\int S(E)\ \phi_E(E)\ \mathrm{d}E} \tag{6}$$

where $\phi_E(E)$ represents again the spectral fluence.

Connection between restricted and unrestricted dose-averaged LET

If we consider a virtual site that is infinitely large to contain all the energy lost by the particle, then $\Delta \to \infty$, and $d\varepsilon_\infty$ in equation (5) coincides with the microdosimetric mean energy imparted, $\overline{\varepsilon_s} \to d\varepsilon_\infty$. This situation occurs as long as secondary electrons do not travel a distance from the primary track comparable with the dimensions of the site. Equivalently, if a virtual site infinitely small is considered, then $\bar{s} \to 0$. In practice, this happens if stopping value does not appreciably change along the path of the particle within the site. Now, in the case of this double-ideally virtual site, equation (6) can be expressed in terms of microdosimetric quantities means as

$$\bar{L}_{\infty,D} = \lim_{\substack{\Delta \to \infty \\ \bar{s} \to 0}} \frac{1}{\bar{s}} \frac{\int \overline{\varepsilon_s}^2(E)\ \phi_E(E)\ \mathrm{d}E}{\int \overline{\varepsilon_s}(E)\ \phi_E(E)\ \mathrm{d}E} = \lim_{\substack{\Delta \to \infty \\ \bar{s} \to 0}} \frac{1}{\bar{s}} \frac{\sigma^2_{\overline{\varepsilon_s}} + \overline{\overline{\varepsilon_s}}^2}{\overline{\overline{\varepsilon_s}}} = \lim_{\substack{\Delta \to \infty \\ \bar{s} \to 0}} \frac{\overline{\overline{\varepsilon_s}}}{\bar{s}} \left(1 + \frac{\sigma^2_{\overline{\varepsilon_s}}}{\overline{\overline{\varepsilon_s}}^2}\right) \tag{7}$$

where we have used the general relation $\sigma^2_x = \overline{x^2} - \bar{x}^2$, applied for the case $x = \overline{\varepsilon_s}$, so that we have $\overline{\overline{\varepsilon_s}^2} = \sigma^2_{\overline{\varepsilon_s}} + \overline{\overline{\varepsilon_s}}^2$.

As, by definition, $\bar{L}_{\infty,D} = \lim_{\substack{\Delta \to \infty \\ \bar{s} \to 0}} \bar{L}_{\Delta,D}$, it follows

$$\bar{L}_{\Delta,D} = \frac{\overline{\overline{\varepsilon_s}}}{\bar{s}} \left(1 + \frac{\sigma^2_{\overline{\varepsilon_s}}}{\overline{\overline{\varepsilon_s}}^2}\right). \tag{8}$$

Note that the microscopic spatially-restricted $\bar{L}_{\Delta,D}$ from equation (8) will differ from the macroscopic unrestricted $\bar{L}_{\infty,D}$ in equation (7) as much as the real microdosimetric site considered deviates from the doubly ideal situation represented by the twofold limit in equation (7). The expression in equation (8) according to the equations (3) and (4), only needs two microdosimetric energy-dependent functions: the average energy imparted per event $\overline{\varepsilon_s}(E)$ and the average segment length $\bar{s}(E)$, instead of the six functions necessary to compute $\bar{L}_{\Delta,D}$ through equation (2). Note that, according to y definition in equation (1), the expression for $\bar{y}_D \equiv \bar{y}_F(1 + \sigma^2_y/\bar{y}^2_F)$ is quite similar to equation (8):

$$\bar{y}_D \equiv \frac{\overline{\overline{\varepsilon_s}}}{\bar{\bar{s}}} \left(1 + \frac{\sigma^2_{\varepsilon_s,\phi}}{\overline{\overline{\varepsilon_s}}^2}\right) = \frac{\overline{\overline{\varepsilon_s}}}{\bar{\bar{s}}} \left(1 + \frac{\overline{\sigma^2_{\varepsilon_s}} + \sigma^2_{\overline{\varepsilon_s}}}{\overline{\overline{\varepsilon_s}}^2}\right) \tag{9}$$

where the second equality is obtained directly from equation (4) and segment length is now double-averaged to take into account the most general case, in which it can depend on the particle energy: $\bar{\bar{s}} = \int \bar{s}(E)\ \phi_E(E)\ \mathrm{d}E$. However, this can be approximated by simply $\bar{s}$ as long as the fraction of particles with range shorter than the site

dimension is negligible, which turns out to be most of the cases for typical energies and site dimensions in proton radiotherapy. Under this assumption, an expression for δ_2 can be obtained from equations (2), (8) and (9) as

$$\delta_2 = \frac{\overline{\sigma^2_{\varepsilon_s}}}{\overline{\overline{\varepsilon_s}}} - \frac{\sigma^2_s}{\bar{s}^2}\left(\overline{\overline{\varepsilon_s}} + \frac{\sigma^2_{\overline{\varepsilon_s}}}{\overline{\overline{\varepsilon_s}}}\right). \tag{10}$$

As seen in equation (8) a third microdosimetric energy-dependent function needs to be incorporated to consider the spread of the energy imparted around its mean value: the variance of the energy imparted per event $\sigma^2_\varepsilon(E)$-or, equivalently, its squared root–.

Revision of the needed microdosimetric functions to be modeled

In Bertolet *et al* (2019a) we presented analytical models to recreate the microdosimetric quantities correspondent to different monoenergetic proton beams. The microdosimetric patterns of energy deposition were obtained by using MC simulations, done with Geant4-DNA, of monoenergetic proton beams up to 100 MeV penetrating into spherical sites of 1 μm, 5 μm and 10 μm in-diameter. From these results, a series of analytical functions of the beam energy were derived. Namely, analytical forms for those site dimensions were obtained for the quantities $\bar{\varepsilon}_s(E)$, $\sigma_{\varepsilon_s}(E)$, $\bar{s}(E)$, $\bar{s}_D(E)$, $\delta_1(E)$ and $\sigma_\delta(E)$, where the two latter are the average and standard deviation of the distribution of energy imparted per collision, respectively. Note that, as shown in that work, $\delta_2 = \delta_1\,(1 + \sigma^2_\delta/\delta^2_1)$ and, therefore, from the six previous functions, it is possible to calculate $\bar{L}_{\Delta,D}$ according to equation (2).

Now, according to equation (8), three functions modelled in that work are not necessary anymore: $\bar{s}_D(E)$, $\delta_1(E)$ and $\sigma_\delta(E)$, being the latter two the average and standard deviation of the distribution of energy imparted per collision, respectively. This is especially convenient since that distribution needs to be obtained from mono-energetic independent simulations (Bertolet *et al* 2019b). In this work, we show that equation (8) is equivalent to equation (2) to obtain restricted LETd from microdosimetry in a more efficient and compact way.

Furthermore, we calculate three-dimensional distributions of $\bar{y}_D$ according to equation (9). The interest on $\bar{y}_D$ is twofold: first, $\bar{y}_D$ is a measurable quantity as long as a microdosimeter capable to store energy deposition distributions is available, while $\bar{L}_{\Delta,D}$ is not. This can be understood just looking at the difference between equations (8) and (9): $\sigma^2_{\varepsilon_s}$ is the actual variance of the measured distribution whereas $\sigma^2_{\overline{\varepsilon_s}}$ is the variance of the mean energies imparted if the problem is decomposed in its spectral components, which needs the knowledge of the specific energetic spectrum measured by the microdosimeter. Second, as it has been pointed out (Grassberger and Paganetti 2011), $\bar{y}_D$ can be a more representative quantity to characterize the energy imparted and eventual biological damage in patients than $\bar{L}_{\Delta,D}$, which, indeed, disregards the volumetric pattern of deposition of energy reducing the problem to a unidimensional one. Nevertheless, as multiple models for biological effect are based on LETd, we keep calculating this quantity in its two versions, unrestricted and restricted; their differences between each other and with respect to $\bar{y}_D$ are here explored.

MicroCalc: an analytical algorithm based on spectral fluence models

In order to obtain the integrations over the spectrum given in equations (3), (4) and (6), we have developed an analytical algorithm to reproduce the spectra at the voxel level in proton particle therapy. This algorithm has been presented in previous articles (Bertolet *et al* 2019c, 2020), in which calculations of unrestricted LETd as well as dose are shown and benchmarked against Monte Carlo computations, and can be briefly summarized as follows:

Transport of monoenergetic proton beams with energies in the clinical range (50–250 MeV) in water was calculated by means of MC simulations. Different types of particles are separated depending on their spectra: primary protons, secondary protons and other secondary particles. The dependency of the fluence of each one both on depth and laterally was modeled using analytical functions. At the same time, spectra for each one is assumed to be Gaussian and the mean and the standard deviation of these Gaussian spectra are, respectively, analytically modeled as functions of the depth and the lateral distance to the beam axis. The combination of these two models yields the spectral fluence for each species. Then, the integration given in equation (6) can be performed for each one of the species. The average LET is obtained as the fluence-weighted average of these results. More details can be obtained elsewhere (Bertolet *et al* 2020).

Here, we reproduce the unrestricted LETd calculation done in Bertolet *et al* (2020). The above algorithm is now used to obtain $\phi_E(E)$ at each position to perform the integrations in equations (3) and (4) to eventually calculate restricted LETd and $\bar{y}_D$ for spherical sites of 1 μm and 10 μm using the microdosimetric functions developed in Bertolet *et al* (2019a). These functions are valid up to a beam energy of 100 MeV, being extrapolated beyond this point. The algorithm is already deployed as a script in the treatment planning system (TPS) Eclipse v15.6 of Varian Medical Systems, which allows for calculations in clinical cases. This script is used to produce results for: (i) $\bar{L}_{\Delta,\,D}$ according to equation (2) and to equation (8); (ii) $\bar{L}_{\infty,D}$ according to equation (6); and (iii) $\bar{y}_D$ according to equation (9).

To assess the equivalency between equations (2) and (8), a simple case is evaluated: a pristine Bragg peak for a beam with nominal energy equal to 100 MeV produced with the Ion Beam Applications (IBA) Pencil Beam

Scanning (PBS) system installed in Roberts Proton Center at the Hospital of the University of Pennsylvania. This energy is selected to disregard possible discrepancies coming from the extrapolation of the microdosimetric functions for beam energies beyond 100 MeV.

On the other hand, a prostate cancer clinical case is considered to illustrate and analyze the different distributions of unrestricted LETd, restricted LETd and $\bar{y}_D$. The calculated plan consists of two lateral beams optimized individually to produce a uniform dose distribution over the target, with a prescription dose of 70.2 Gy in 39 fractions. Although MicroCalc considers non-homogeneities in the fluence model, results for $\bar{L}_{\Delta,\ D}$, $\bar{L}_{\infty,D}$ and $\bar{y}_D$ are referred to water. Additionally, results shown here only encompass primary and secondary protons.

Results

Figure 1 shows the profiles for LETd at the central axis for a beam of 100 MeV as nominal energy as well as for a SOBP beam with range 20 cm and 10 cm of modulation. Three different calculations are presented: unrestricted LETd or $\bar{L}_{\infty,\ D}$ according to equation (6) and restricted $\bar{L}_{\Delta,D}$ for two different microdosimetric sites, both spherical and with diameter of 1 μm and 10 μm, respectively. Results corresponding to equations (2) and (8) are compared to assess the equivalency of the methods. The mean difference along the profiles taking samples stepped by 1 mm, between these two curves, are 0.05 ± 0.04 keV μm^{-1} for the 1 μm case and 0.05 ± 0.02 keV μm^{-1} for the 10 μm case, respectively, where the uncertainties correspond to the standard deviation of the difference samples.

Differences between $\bar{y}_D$ and both versions of LETd are illustrated in figure 2 for the same 100 MeV proton beam. While $\bar{L}_{\Delta,D}$ remains almost independent of the site dimension, $\bar{y}_D$ is clearly higher for the 1 μm case than for the 10 μm case.

An axial plane at the middle of the prostate is selected to show the computed distributions. Dose and unrestricted LETd are the same for the two considered sites, meanwhile restricted LETd and $\bar{y}_D$ distributions are different depending on the site dimension selected. Figure 3 shows the projection of the mentioned distributions upon the chosen axial plane.

The profiles along the dashed line marked in figure 3(a) for these quantities are shown in figure 4. Two types of comparisons are shown: on the one hand, restricted and unrestricted LETd are displayed in figure 4(a). Unrestricted LETd is markedly higher along the whole profile than both restricted versions of LETd, being the 10 μm-site-restricted LETd curve slightly above the 1 μm-site-restricted LETd. On the other hand, figure 4(b) shows the differences between unrestricted LETd and $\bar{y}_D$. In this case, $\bar{y}_D$ for the site of 1 μm in diameter is clearly superior to $\bar{y}_D$ for the site of 10 μm. As expected according to equations (2) and (9), $\bar{y}_D$ curve is above $\bar{L}_D$ curves at every point. To evaluate the relative shape of each distribution, the ratio between the peaks and the plateau, at the center of the profiles, yields the values: (a) 1.90 for $\bar{L}_{\infty,D}$; (b) 2.17 for $\bar{L}_{\Delta,D}$ (1 μm); (c) 2.15 for $\bar{L}_{\Delta,D}$ (10 μm); 1.78 for y_D (1 μm); and 2.01 for y_D (10 μm).

Discussion

Results in figure 1 seem to endorse the expression for restricted LETd from microdosimetry given in equation (8). Although both calculations share, essentially, the models for single-event average energy imparted per event $\bar{\varepsilon}(E)$ and mean segment length $\bar{s}(E)$, the use of equation (2) includes the other four quantities modelled in Bertolet *et al* (2019a), i.e. standard deviation for the single-event energy imparted in the site $\sigma_\varepsilon(E)$, weighted-mean segment length $\bar{s}_D(E)$ and average and standard deviation for the energy imparted in the site per collision, $\delta_1(E)$ and $\sigma_\delta(E)$, respectively. These latter two are obtained from independent MC simulations (Bertolet *et al* 2019b), making results from equations (2) and (8) independent as well. Since our models were developed up to 100 MeV, it looks fair to restrict the comparison between these two equations until that limit. Otherwise, spurious differences due to extrapolations of the different functions would miss-represent the equivalency of the two equations.

Although results here shown only consider primary and secondary protons, disregarding the contribution from heavier nuclear fragments, our algorithm allows for further incorporation of different particle species, as shown in Bertolet *et al* (2020). The process to add the contribution from any other particle p is essentially the same as for protons: (a) model the spectral fluence $\phi_E(E;p)$; and (b) model the microdosimetry patterns of energy deposition, characterized by the functions $\bar{\varepsilon}_s(E;p)$, $\sigma^2_{\varepsilon_s}(E;p)$, etc. No other particles apart from protons are here considered because of simplicity. Comparative analysis between relative $\bar{y}_D$, $\bar{L}_{\infty,D}$ and $\bar{L}_{\Delta,D}$ is expected to stand as valid, since other particles' contributions should affect similarly to the three quantities. However, if absolute values of any of these quantities are applied to clinical models, relevant contributions from other particles, such as alpha particles and deuterons (Grassberger and Paganetti 2011), need to be included in the calculation. Thus, a limitation of this work in its current version is the lack of consideration for these secondary contributions.

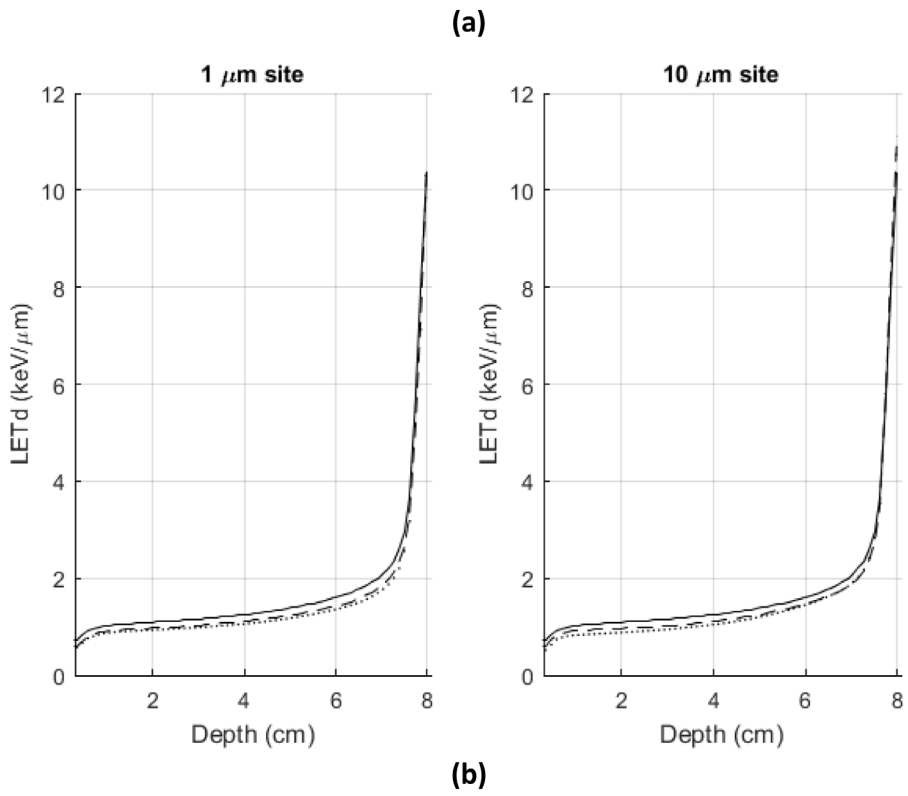

Figure 1. Profiles at the central axis for unrestricted LETd and restricted LETd calculations using the MicroCalc algorithm and considering only primary and secondary protons, using equation (6) for unrestricted LETd, and (2) and (8) for restricted LETd, respectively for a beam with nominal energy equal to 100 MeV. Left panel is obtained using the microdosimetric models for spherical sites of 1 μm in diameter meanwhile right panel shows the same results for spherical sites of 10 μm in diameter. Legends: ——— $\bar{L}_{\infty,D}$ from equation (6); ..... $\bar{L}_{\Delta,D}$ from equation (2); – – – $\bar{L}_{\Delta,D}$ from equation (8).

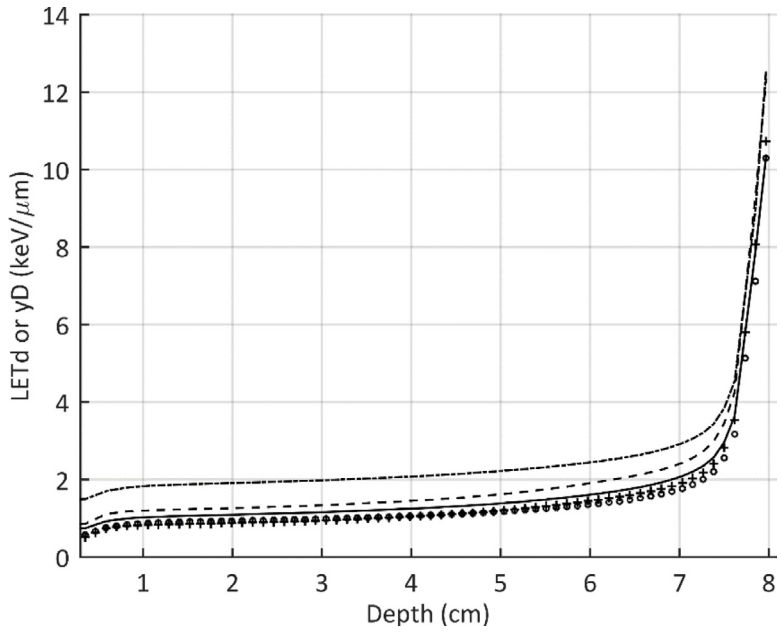

Figure 2. Profiles at the central axis for unrestricted LETd, restricted LETd and dose-mean lineal energy for two different microdosimetric sites, spheres with diameters of 1 μm and 10 μm, for a 100 MeV beam considering only primary protons and secondary protons. Unrestricted LETd, restricted LETd and $\bar{y}_D$ are calculated according to equations (6), (8) and (9), respectively. Legends: ——— $\bar{L}_{\infty,D}$; ooooo $\bar{L}_{\Delta,D}$- 1 μm site; +++ + + $\bar{L}_{\Delta,D}$- 10 μm site; – – – – $\bar{y}_D$-1 μm site; – – – $\bar{y}_D$-10 μm site.

All results here shown are reported in terms of energy imparted to liquid water. Unrestricted LET in terms of energy imparted to other media can be obtained by using the stopping power ratio for each energy integrated along the pre-calculated beam spectrum. However, the correct calculations of restricted LET and microdosimetric quantities would require models for the functions $\bar{\varepsilon}(E)$, $\sigma^2_{\varepsilon}(E)$, etc after MC simulations in those media. This

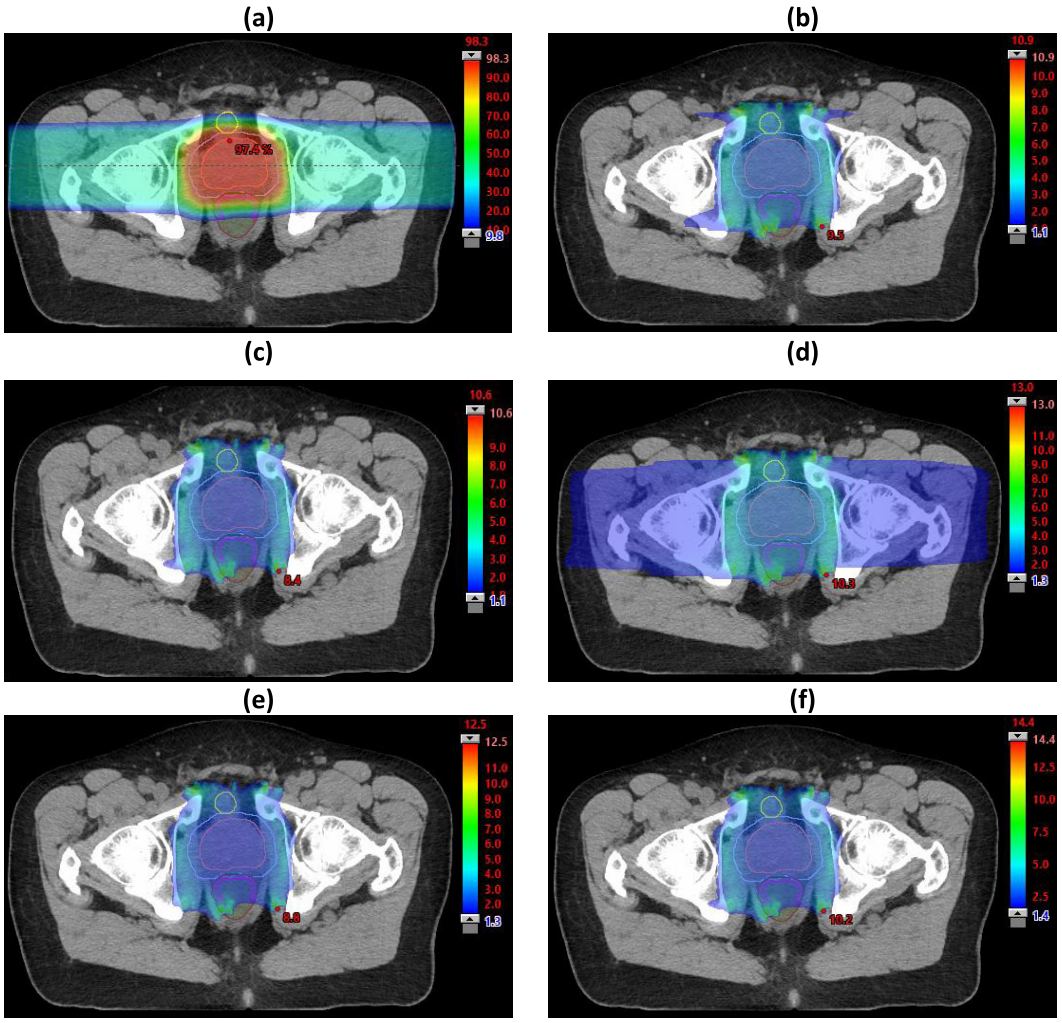

Figure 3. Projections of the calculated distributions with the MicroCalc algorithm as a script in Eclipse for (a) dose; (b) $\bar{L}_{\infty,D}$; (c) $\bar{L}_{\Delta,\ D}$-1 μm site; (d) $\bar{y}_D$-1 μm site; (e) $\bar{L}_{\Delta,\ D}$-10 μm site; and (f) $\bar{y}_D$-10 μm site on an axial plane for a prostate cancer clinical case with two lateral beams. $\bar{L}_{\Delta,\ D}$ distributions are calculated using equation (8). Structures present in this plane are represented by color lines: CTV—orange; PTV—purple; Bladder—yellow; Whole rectum—brown; Rectal anterior wall—pink. Color maps represent, in each case, the values given by the scale at the right of the figures. The maximum value for the plane is indicated in red in keV μm^{-1}, except for the dose distribution (a), in which case is given in percentage of dose prescription. The dashed line in the dose distribution (a) indicates the position of the lateral profiles shown in figure 4.

represents another limitation of our method for now, although it is a potential future improvement to implement. In any case, the trends observed here are not expected to be substantially different, thus we can use similar concepts for such improvements.

Restricted LETd is logically below unrestricted LETd, although no great differences are observed between the restrictions for 1 μm and for 10 μm. Differences between restricted and unrestricted LETd tend to disappear when LET grows, i.e. near the end of the range, due to the short range of the secondary electrons around the proton track. However, when superposing beams, as in figures 3 and 4, restriction on the energy has an impact on the curves for $\bar{L}_{\Delta,D}$ due to the contribution from the low LET part of each beam to the high LET part (end of the range) of the opposing beam. This effect also produces the different ratio peak-plateau in the sagittal profiles for the two opposed beams in figure 4 for restricted and unrestricted LETd.

An important element to the discussion of the results is related to the use of these parameters for biophysical optimization of proton plans. Whether they all equivalent or there is a more optimal configuration, it is logical to think that, if biological damage (end point) is related to the deposition of energy in a given volume, the specification of the dose quality inducing such effect should reflect the dimension of the volume, and for that reason restricted magnitudes should be better equipped to represent optimization biological damage that ultimately should represent an increase of the therapeutic window. Furthermore, when considering the difference in peak-to-plateau ratios, it seems that restricted LET provides the highest ratios, which translates into this parameter providing the highest gradients for biophysical optimization purposes. However, previous works (Grassberger *et al* 2011) have indicated that $\bar{y}_D$ would be a more representative quantity to characterize biological effect.

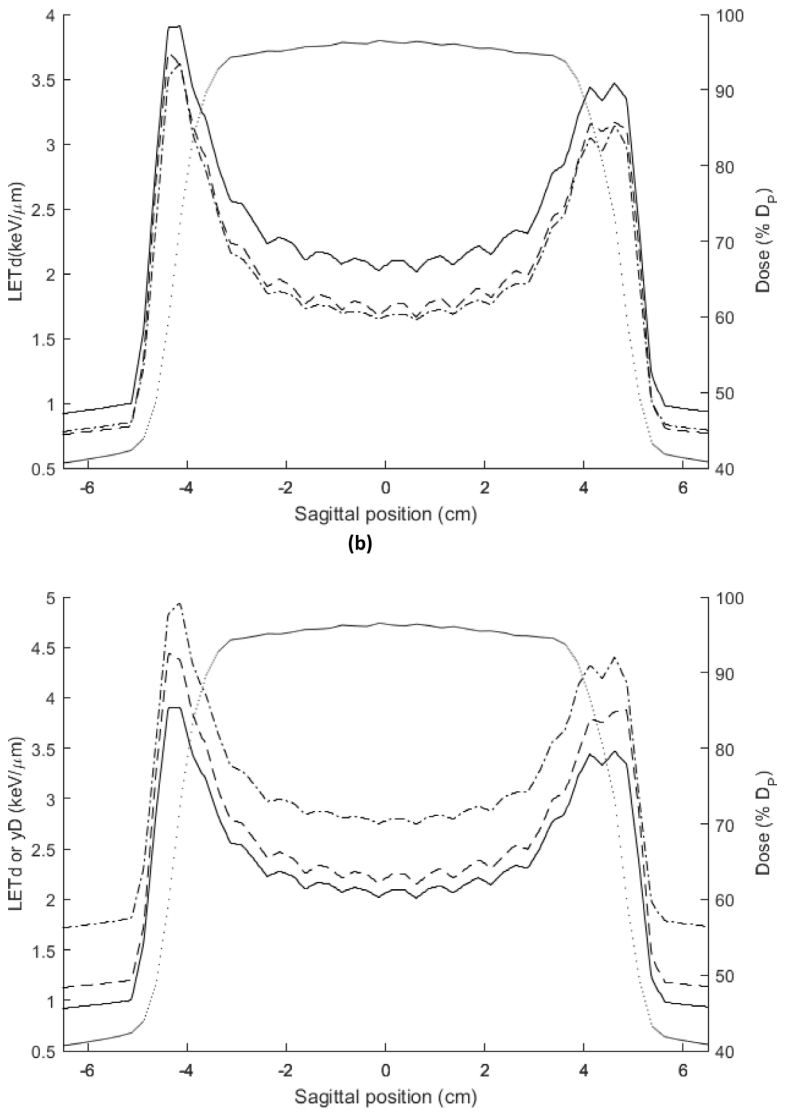

Figure 4. Sagittal profiles for the distributions in the prostate case shown in figure 3. (a) Profiles for unrestricted LETd and restricted LETd; and (b) profiles for unrestricted LETd and $\bar{y}_D$ for spherical sites of 1 μm and 10 μm in diameter. In both cases, the dose profile is also shown. Legends: (a): ..... Dose; ——— $L_{\infty,D}$; ----- $L_{\Delta,D}$- 1 μm site; – – – $L_{\Delta,D}$-10 μm site. (b) ..... Dose; ——— $L_{\infty,D}$; ----- $\bar{y}_D$-1 μm site; – – – $\bar{y}_D$-10 μm site.

Looking at equation (9), it can be argued that while $\bar{y}_D$ includes: (a) the variability in the energy imparted in a site for a monoenergetic beam, due to straggling and chord length variability, expressed in the term $\overline{\sigma^2_{\varepsilon_s}}$; and (b) the variability in the energy imparted due to different beam energies, i.e. beams with different LET, given by the term $\sigma^2_{\bar{\varepsilon}_s}$. On the other hand, as expectable, $\bar{L}_{\Delta,D}$ only includes the last term, associated to LET variability, according to equation (8). Thus, δ_2 can be calculated in equation (10), obtained by comparing equations (2), (8) and (9) without need for specific MC simulations, as done so far.

The extra term $\overline{\sigma^2_{\varepsilon_s}}$ in $\bar{y}_D$ with respect to $\bar{L}_{\Delta,D}$ justifies that the first one is larger than the second one in figures 2–4. As mentioned, this term is related to the variability on the energy imparted in a site even when there is no LET variability, i.e. due to energy straggling and different chord lengths in each event. The magnitude of the difference between $\bar{y}_D$ and LETd is thus related to the relative relevancy of those two effects with respect to the variability on particles' LET itself. As LET becomes more spread near the end of the range, its relative importance against the other two effects increases so that $\bar{y}_D$ tends to approximate LETd. Additionally, $\bar{y}_D$ is considerably higher for the smaller site (1 μm) than for the 10 μm-site. This can be explained using the same reasoning: the smaller the site, the more relevant energy straggling becomes with respect to LET variability. This result can be turned around by saying $\bar{y}_D$ tends to restrict LETd as the site dimension increases, so at the macroscopic level, they both coincide.

These considerations should be taken into account when performing experimental measurements for LETd. Usual microdosimeters (Lindborg and Waker 2017) as tissue-equivalent proportional counters (TEPC) or silicon-based diodes, collect distributions of energy imparted without the ability to discriminate the energetic

spectrum so that the distinction between variance terms given in equation (3) is not available. Therefore, they provide $\bar{y}_D$ measurements according to equation (9) and, consequently, the expectable value for that quantity should be—for considerably small devices—higher than the traditionally calculated unrestricted LETd. Nonetheless, our calculation provides with actual values for $\bar{y}_D$ and $\bar{L}_{\infty,\,D}$ so that difference can be assessed in a straightforward way without needing the knowledge of the energy spectrum.

Finally, the calculation of RBE from the physical quantities computed here is beyond the scope of this work. However, our method is qualified to produce a number of distributions for different quantities directly related with already stablished RBE models. Indeed, not only track-related quantities as the three presented here can be computed from the microdosimetric models: weighted-average specific energy, $\bar{z}_D$ may be obtained from the $\bar{\varepsilon}(E)$ function with an expression similar to equation (9), as well as combinations of these quantities. As there are RBE models based on $\bar{z}_D$ published in the literature (Kase *et al* 2006, Inaniwa *et al* 2018), this puts forward the possibility of deployments of new models for analytical calculations of RBE in a TPS.

Conclusions

Unrestricted LETd, restricted LETd and $\bar{y}_D$ 3D distributions in clinical cases are analytically computable by using a fluence-based algorithm in combination with our models for microdosimetric functions dependent on the energy. These three distributions are similar, but differences can be observed depending on the size of the microdosimetric site considered. Particularly, $\bar{y}_D$ and LETd are more different as the microdosimetric site becomes smaller. This work provides direct distributions of $\bar{y}_D$ that can be compared with experimental measurements and, at the same time, opens the possibility of using microdosimetric derived quantities –restricted LETd and $\bar{y}_D$—to drive biophysical optimization in proton therapy treatments as well as further development of RBE models for RBE based on them.

Acknowledgments

This project is supported by Varian Medical Systems, Palo Alto, California; M A Cortés-Giraldo has been funded by the Spanish Government under Grant No. RTI2018-098117-B-C21.

Appendix. Demonstration of equation (4)

According to equation (4), the variance of the weighted sum of distributions dependent on the same variable is the mean of the variances of each individual distribution plus the variance of the means of the individual distributions around the global mean. To prove this, let us consider, for the sake of simplicity, just two distributions dependent on the variable x, $f_1(x)$ and $f_2(x)$, and a weighted sum of them:

$$F(x) = \omega_1 f_1(x) + \omega_2 f_2(x) \tag{A.1}$$

with the condition $\omega_1 + \omega_2 = 1$. The mean of the individual and the averaged distributions is, respectively:

$$\bar{x}_1 = \int x\, f_1(x)\, \mathrm{d}x, \tag{A.2}$$

$$\bar{x}_2 = \int x\, f_2(x)\, \mathrm{d}x, \tag{A.3}$$

and

$$\bar{x}_F = \int x\, F(x)\ \mathrm{d}x = \omega_1 \bar{x}_1 + \omega_2 \bar{x}_2 \tag{A.4}$$

as shown in equation (3). The variances of these three distributions are, respectively:

$$\sigma_1^2 = \int x^2\, f_1(x)\, \mathrm{d}x - \bar{x}_1^2 = \overline{x_1^2} - \bar{x}_1^2, \tag{A.5}$$

$$\sigma_2^2 = \int x^2\ \ f_2(x)\ \ \mathrm{d}x - \bar{x}_2^2 = \overline{x_2^2} - \bar{x}_2^2, \tag{A.6}$$

and

$$\sigma_F^2 = \int x^2\ F(x)\, \mathrm{d}x - \bar{x}_F^2 = \omega_1 \overline{x_1^2} + \omega_2 \overline{x_2^2} - (\omega_1 \bar{x}_1 + \omega_2 \bar{x}_2)^2. \tag{A.7}$$

Using equations (A.5)–(A.7) becomes

$$\sigma_F^2 = \omega_1\sigma_1^2 + \omega_2\sigma_2^2 + \left(\omega_1 - \omega_1^2\right)\bar{x}_1^2 + \left(\omega_2 - \omega_2^2\right)\bar{x}_2^2 - 2\omega_1\omega_2\bar{x}_1\bar{x}_2. \tag{A.8}$$

On the one hand, the first two terms summed correspond to the mean of the individual variances, $\overline{\sigma_x^2} = \omega_1\sigma_1^2 + \omega_2\sigma_2^2$. On the other hand, the variance of the individual means around the global mean $\bar{x}_F$ is

$$\sigma_{\bar{x}}^2 = \omega_1(\bar{x}_1 - \bar{x}_F)^2 + \omega_2(\bar{x}_2 - \bar{x}_F)^2 = \omega_1\bar{x}_1^2 + \omega_2\bar{x}_2^2 + (\omega_1 + \omega_2)\bar{x}_F^2 - 2\bar{x}_F(\omega_1\bar{x}_1 + \omega_2\bar{x}_2) \tag{A.9}$$

where using equation (A.4) and the condition $\omega_1 + \omega_2 = 1$, it follows

$$\sigma_{\bar{x}}^2 = \omega_1\bar{x}_1^2 + \omega_2\bar{x}_2^2 - \bar{x}_F^2 = \left(\omega_1 - \omega_1^2\right)\bar{x}_1^2 + \left(\omega_2 - \omega_2^2\right)\bar{x}_2^2 - 2\omega_1\omega_2\bar{x}_1\bar{x}_2 \tag{A.10}$$

where the last equality is obtained by substituting $\bar{x}_F$ by its expression in equation (A.4). This expression coincides with the last term in equation (A.8), so that we can conclude

$$\sigma_F^2 = \overline{\sigma_x^2} + \sigma_{\bar{x}}^2 \tag{A.11}$$

result which is recursively applicable to a sum of an arbitrary number of distributions, as long as the resulting distribution is normalized (i.e. the condition $\sum\omega_i = 1$ is required). This is done in equation (4) by introducing the denominator $\int \phi_E(E)\ \mathrm{d}E$, that ensures that the resulting distribution is normalized.

ORCID iDs

A Bertolet https://orcid.org/0000-0002-9890-693X
M A Cortés-Giraldo https://orcid.org/0000-0002-3646-1015

References

An Y *et al* 2017 Robust intensity-modulated proton therapy to reduce high linear energy transfer in organs at risk *Med. Phys.* **44** 6138–47
Bertolet A *et al* 2019a Segment-averaged LET concept and analytical calculation from microdosimetric quantities in proton radiation therapy *Med. Phys.* **46** 4204–14
Bertolet A *et al* 2019c Calculation of clinical dose distributions in proton therapy from microdosimetry *Med. Phys.* **46** 5816–23
Bertolet A, Baratto-Roldán A, Barbieri S, Baiocco G, Carabe A and Cortés-Giraldo M A 2019b Dose-averaged LET calculation for proton track segments using microdosimetric Monte Carlo simulations *Med. Phys.* **46** 4184–92
Bertolet A, Cortés-Giraldo M A, Souris K and Carabe A 2020 A kernel-based algorithm for the spectral fluence of clinical proton beams to calculate dose-averaged LET and other dosimetric quantities of interest *Med. Phys.* (accepted) (https://doi.org/10.1002/mp.14108)
Cao W *et al* 2018 Linear energy transfer incorporated intensity modulated proton therapy optimization *Phys. Med. Biol.* **63** 015013
Cortés-Giraldo M A and Carabe A 2015 A critical study of different Monte Carlo scoring methods of dose average linear-energy-transfer maps calculated in voxelized geometries irradiated with clinical proton beams *Phys. Med. Biol.* **60** 2645–69
Deng W *et al* 2019 Hybrid 3D analytical linear energy transfer calculation algorithm based on precalculated data from Monte Carlo simulations *Med. Phys.* **47** 745–52
Fager M *et al* 2015 Linear energy transfer painting with proton therapy: a means of reducing radiation doses with equivalent clinical effectiveness *Int. J. Radiat. Oncol.* **91** 1057–64
Giantsoudi D, Grassberger C, Craft D, Niemierko A, Trofimov A and Paganetti H 2013 Linear energy transfer-guided optimization in intensity modulated proton therapy: feasibility study and clinical potential *Int. J. Radiat. Oncol. Biol. Phys.* **87** 216–22
Grassberger C and Paganetti H 2011 Elevated LET components in clinical proton beams *Phys. Med. Biol.* **56** 6677–91
Grassberger C, Trofimov A, Lomax A and Paganetti H 2011 Variations in linear energy transfer within clinical proton therapy fields and the potential for biological treatment planning *Int. J. Radiat. Oncol. Biol. Phys.* **80** 1559–66
Guan F *et al* 2019 RBE model-based biological dose optimization for proton radiobiology studies *Int. J. Part. Ther.* **5** 160–71
Hawkins R B 1996 A microdosimetric-kinetic model of cell death from exposure to ionizing radiation of any LET, with experimental and clinical applications *Int. J. Radiat. Biol.* **69** 739–55
Hawkins R B 2003 A microdosimetric-kinetic model for the effect of non-poisson distribution of lethal lesions on the variation of RBE with LET *Radiat. Res.* **160** 61–9
ICRU 1983 *Report 36. Microdosimetry* (Bethesda, MD: ICRU)
ICRU 2016 *Report 90: Key Data for Ionizing Radiation Dosimetry: Measurement Standards and Applications* vol 14 (Bethesda, MD: ICRU)
Inaniwa T, Kanematsu N and Inaniwa T 2018 Adaptation of stochastic microdosimetric kinetic model for charged-particle therapy treatment planning *Phys. Med. Biol.* **63** 0–17
Inaniwa T, Kanematsu N, Noda K and Kamada T 2017 Treatment planning of intensity modulated composite particle therapy with dose and linear energy transfer optimization *Phys. Med. Biol.* **62** 5180–97
Kase Y *et al* 2006 Microdosimetric measurements and estimation of human cell survival for heavy-ion beams *Radiat. Res.* **166** 629–38
Kase Y *et al* 2013 Microdosimetric calculation of relative biological effectiveness for design of therapeutic proton beams *J. Radiat. Res.* **54** 485–93
Kase Y, Kanai T, Matsufuji N, Furusawa Y, Elsässer T and Scholz M 2008 Biophysical calculation of cell survival probabilities using amorphous track structure models for heavy-ion irradiation *Phys. Med. Biol.* **53** 37–59
Kellerer A M 1985 Fundamentals of microdosimetry *The Dosimetry of Ionization Radiation* vol I, ed K R Kase *et al* (New York: Academic) pp 77–162
Lindborg L and Waker A 2017 *Microdosimetry. Experimental Methods and Applications* (Boca Raton, FL: CRC Press)
Marsolat F, De Marzi L, Pouzoulet F and Mazal A 2016 Analytical linear energy transfer model including secondary particles: calculations along the central axis of the proton pencil beam *Phys. Med. Biol.* **61** 740–57

McMahon S J and Paganetti H 2018 Prise KM. LET-weighted doses effectively reduce biological variability in proton radiotherapy planning *Phys. Med. Biol.* **63** 225009

Newpower M *et al* 2019 Using the proton energy spectrum and microdosimetry to model proton relative biological effectiveness *Int. J. Radiat. Oncol. Biol. Phys.* **104** 316–24

Paganetti H 2014 Relative biological effectiveness (RBE) values for proton beam therapy. Variations as a function of biological endpoint, dose, and linear energy transfer *Phys. Med. Biol.* **59** R419–72

Paganetti H *et al* 2019 Report of the AAPM TG-256 on the relative biological effectiveness of proton beams in radiation therapy *Med. Phys.* **46** e53–78

Peeler C R *et al* 2016 Clinical evidence of variable proton biological effectiveness in pediatric patients treated for ependymoma *Radiother. Oncol.* **121** 395–401

Perales Á, Baratto-Roldán A, Kimstrand P, Cortés-Giraldo M A and Carabe A 2019 Parameterising microdosimetric distributions of mono-energetic proton beams for fast estimates of y_D and y^* *Biomed. Phys. Eng. Express* **5** 045014

Romano F *et al* 2014 A Monte Carlo study for the calculation of the average linear energy transfer (LET) distributions for a clinical proton beam line and a radiobiological carbon ion beam line *Phys. Med. Biol.* **59** 2863–82

Sánchez-Parcerisa D, López-Aguirre M, Dolcet Llerena A, Udías J M, Llerena A D and Ud M 2019 MultiRBE: treatment planning for protons with selective radiobiological effectiveness *Med. Phys.* **46** 4276–84

Unkelbach J, Botas P, Giantsoudi D, Gorissen B L and Paganetti H 2016 Reoptimization of intensity modulated proton therapy plans based on linear energy transfer *Int. J. Radiat. Oncol. Biol. Phys.* **96** 1097–106

Wilkens J J and Oelfke U 2003 Analytical linear energy transfer calculations for proton therapy *Med. Phys.* **30** 806–15

Wilkens J J and Oelfke U 2004 Three-dimensional LET calculations for treatment planning of proton therapy *Z. Med. Phys.* **14** 41–6